Lateral uniformity of India Plate strength over central and eastern Nepal

Theo Berthet, Gyoergy Hetenyi, Rodolphe Cattin, Soma Nath Sapkota, Cedric Champollion, Thakur Kandel, Erik Doerflinger, Dowchu Drukpa, Sarah Lechmann, Mickael Bonnin

Geophysical Journal International

Geophys. J. Int. (2013) **195,** 1481–1493
Advance Access publication 2013 September 27

doi: 10.1093/gji/ggt357

Lateral uniformity of India Plate strength over central and eastern Nepal

Théo Berthet,[1] György Hetényi,[2] Rodolphe Cattin,[1] Soma Nath Sapkota,[5] Cédric Champollion,[1] Thakur Kandel,[5] Erik Doerflinger,[1] Dowchu Drukpa,[4] Sarah Lechmann[3] and Mickael Bonnin[1]

[1] *Géosciences Montpellier, UMR*5243*, Université Montpellier* 2*, Place E. Bataillon,* 34095 *Montpellier, France. E-mail: theo.berthet@gm.univ-montp2.fr*
[2] *Swiss Seismological Service, Department of Earth Sciences, ETH Zürich, Sonneggstrasse* 5*,* 8092 *Zürich, Switzerland*
[3] *Geological Institute, Department of Earth Sciences, ETH Zürich, Sonneggstrasse* 5*,* 8092 *Zürich,, Switzerland*
[4] *Seismology and Geophysics Division, Department of Geology and Mines, Post Box* 173*, Thimphu, Bhutan*
[5] *National Seismological Centre, Department of Mines and Geology, Lainchur, Kathmandu, Nepal*

Accepted 2013 September 4. Received 2013 September 3; in original form 2012 October 22

SUMMARY

The current understanding of the Himalayan lithosphere stems mostly from cross-sections through the range at the longitude of the Kathmandu Basin. In this paper we laterally extend the analyses of structures and rheology along the Nepal Himalayas between the Pokhara valley and the Arun river. We take advantage of available information and a new data set including gravity measurements and a receiver function profile. It appears that the geometry of the Moho inferred from seismological profiles and long-wavelength gravity anomalies does not exhibit major East–West variations within the 350-km-wide study area. Using thermomechanical modelling, we show that the northward deepening of the Moho observed along profiles perpendicular to the main thrust faults can be interpreted simply as the bending of a strong India Plate. This result suggests a gradual mechanical decoupling between the crust and the mantle, leading to a northward decrease of the effective elastic thickness of the Indian lithosphere from ∼75 km to ∼25 km beneath the Ganga Basin and the Tibetan Plateau, respectively. Our results also confirm (partially) eclogitized lower Indian crust beneath southern Tibet. At shorter wavelengths, the observed gravity profiles exhibit some small lateral variations that can be interpreted in terms of east–west variations of the thickness of subsurface geological structures such as the Ganga Basin and the Tethyan Sedimentary Sequence.

Key words: Gravity anomalies and Earth structure; Continental margins: convergent; Dynamics: gravity and tectonics; Lithospheric flexure; Crustal structure; Rheology: crust and lithosphere.

1 INTRODUCTION

The Himalayan belt along the southern edge of the Tibetan Plateau is one of the most spectacular products of the ongoing collision between India and Eurasia. Over the last four decades many seismological and gravity experiments as well as GPS, structural geology, geomorphology and thermochronological campaigns were conducted in the Himalayas to image its deep structure and understand its dynamics (e.g. Le Fort 1975; Hirn *et al.* 1984; Zhao & Nelson 1993; Brown *et al.* 1996; Alsdorf *et al.* 1998; Cattin *et al.* 2001; Jouanne *et al.* 2004; Schulte-Pelkum *et al.* 2005; Hetényi *et al.* 2006; Nabelek *et al.* 2009; Robert *et al.* 2011). The main features of the collision zone are now relatively well known; beneath the range, the India Plate is bent and underthrusts the southern Tibetan Plateau for about 450 km distance. The thickness of the crust increases by ∼40 km from India to southern Tibet. The shortening is accommodated along major frontal thrust (MFT) faults connected to the Main Himalayan Thrust (MHT), which is a midcrustal reflector imaged at a depth of ∼25 to ∼40 km. However, because most of these available data are located in central Nepal, the current understanding of the Himalayas is mostly limited to the cross-section through the range at the longitude of the Kathmandu Basin. The lateral variation of structures is nevertheless important. First, it helps to unravel the mountain building processes. For instance, along strike variations can reveal rheological contrasts or inherited structures, which can play a major role in the orogenic evolution (Gahalaut & Kundu 2012). Second, to improve seismological hazard assessment due to self-similarity of earthquakes as the magnitude of future

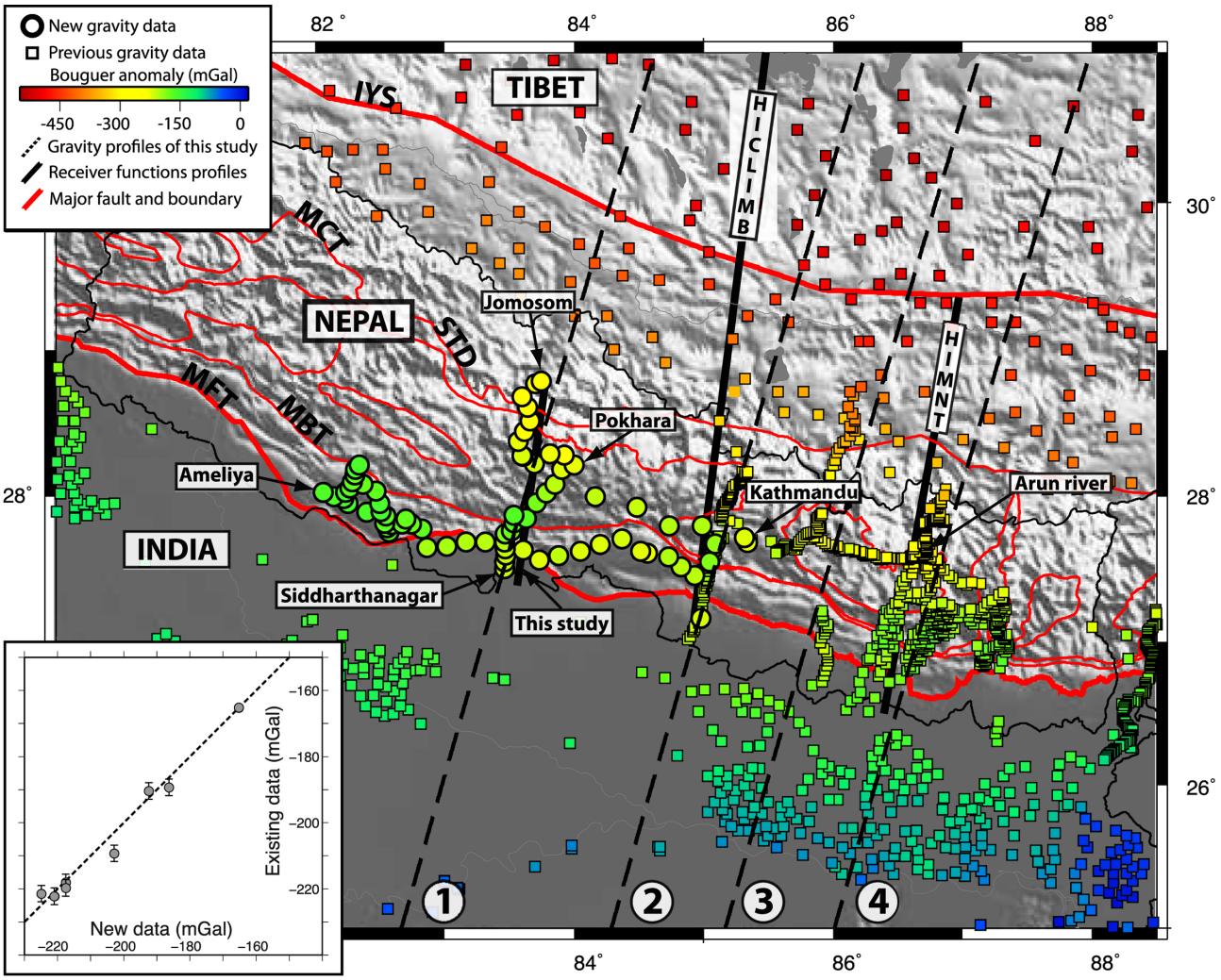

Figure 1. Map of the study area showing gravity data in Nepal, northern India and southern Tibet. Circles represent the location of new gravity measurements and squares the previous data set (from BGI, Cattin *et al.* (2001), Sun (1989) and Tiwari *et al.* (2006)). The colour scale shows Bouguer anomalies in mGal. Also shown are receiver function profiles obtained in eastern Nepal: HIMNT experiment (Schulte-Pelkum *et al.* 2005) and in the Hi-CLIMB experiment's main array (Nabelek *et al.* 2009) along 85°E and at the longitude of Pokhara (this study, Hi-CLIMB experiment's Nepal-Pokhara line). Black dashed lines show the locations of profiles 1 to 4 used in this study. Thick red lines represent major faults. MFT, main frontal thrust; MBT, main boundary thrust; MCT, main central thrust; STD, South Tibetan Detachment; IYS, Indus–Yarlung Suture. Inset in the lower left corner shows the discrepancy between new measurements and existing ones.

events can be estimated from fault lengths. Thus the size of lateral similarities of major structures in a seismically active area may control its seismic potential.

Several studies have recently demonstrated that along strike variations exist between the Nepal and Bhutan Himalayas in topography (Duncan *et al.* 2003) or geometry of the MHT (Robert *et al.* 2011). However, these studies do not exhibit significant lateral variations in the Nepal Himalayas. In central an eastern Nepal, geodetic data also show very little variations (Grandin *et al.* 2012). Due to lack and sparseness of geophysical data and the difficulty to assess the consistency of these different methods, the extent of lateral variations at depth is still unconstrained in Nepal.

Here, using a new data set including gravity measurements and receiver functions (RFs) profiles, we study the lateral variations in terms of behaviour of the India Plate in flexure along the Nepal Himalayas between the Pokhara valley and the Arun river (Fig. 1). After a short description of the study area, we present data acquisition and processing. We then combine them with available data in order to obtain four 1000-km-long profiles within a 350-km-wide area in central and eastern Nepal. We next describe the modelling approach and assumptions. Finally we discuss the different wavelengths of the gravity measurements and our findings in terms of flexure of the India Plate and structural variation along the Nepal Himalayas.

2 GEODYNAMIC SETTING OF THE NEPAL HIMALAYAS

As the entire Himalayan arc, the Nepal Himalayas can be divided into four distinct tectonic units (Fig. 1; e.g. Gansser 1964; Le Fort 1975; Yin 2006). The northernmost zone, known as the Tethyan Sedimentary Series (TSS), consists of Cambrian to Eocene sedimentary and low-grade metamorphic rocks. In Nepal, the TSS has a limited extent except in central Nepal where the best sections can be found in the Annapurna–Dhaulagiri region. The TSS lies between the Indus–Yarlung Suture (IYS), which is the northern limit of the

Himalayas, and the South Tibetan Detachement, a north dipping normal fault, which marks the limit with the underlying Higher Himalaya (HH; Burchfield *et al.* 1992). The HH consists of high-grade metamorphic rocks including gneisses, schists and migmatites. The width of this unit varies along Nepal, it is only a few kilometres where the unit is limited to its root zone like in central Nepal whereas it can reach tens of kilometres where it has overthrusted the Lesser Himalaya (LH) forming series of nappes and klippes in western and eastern Nepal (Upreti 1999; DeCelles *et al.* 2001). The LH underlies the HH along the Main Central Thrust (MCT) and forms a series of duplexes composed of low-grade metasedimentary rocks. In eastern Nepal, the LH is mainly exposed in tectonic windows that cut through the extensive crystalline thrust sheet. In central Nepal, the width of LH reaches 100 km because of the absence of overthrusted HH. Crystalline nappes and klippes reappear in western Nepal. The last unit, composed of Neogene to Quaternary syntectonic clastic sediments, is formed by the Siwalik thrust belt. It lies between the Major Boundary Thrust (MBT) to the North and the MFT, which is the most recently activated one in the sequence (Lave & Avouac 2001). South of the MFT is the undeformed foreland basin with relatively recent sedimentary infill up to 6 km in thickness (Raiverman *et al.* 1983).

The localization of the deformation is now well constrained in central and eastern Nepal. The present day shortening rate of 17.8 ± 0.5 mm yr^{-1} is related to interseismic coupling on the MHT fault (Bilham *et al.* 1997; Larson *et al.* 1999; Jouanne *et al.* 2004; Ader *et al.* 2012). At longer timescales, fluvial terrace analyses and tectonostratigraphic studies give a consistent rate (Lave & Avouac 2000; DeCelles *et al.* 2001; Mugnier & Huyghe 2006), suggesting that the Himalayan arc absorbs about 20 km Myr^{-1} convergence by localized thrusting since mid-Miocene times.

Many structural geology field campaigns as well as several seismological and gravity experiments were performed to infer and image the deep structures of the Himalayas in Nepal, which includes the geometry of major faults and the depth of both the Moho and the foreland sedimentary basin. The three north dipping thrusts of the arc (MCT, MBT, MFT) all root on the MHT (Zhao & Nelson 1993; Nelson *et al.* 1996; Lave & Avouac 2000). The MHT consists of a mid-crustal décollement where the India Plate underthrusts the Himalayas and Tibet. Several studies on the shape of the MHT suggest that a ramp-flat-ramp-flat geometry prevails (e.g. Cattin & Avouac 2000; Avouac *et al.* 2001; Nabelek *et al.* 2009). The first ramp corresponds to the currently active MFT and the second one occurs at mid-crustal depth below the topographic front of the HH.

In the Nepal Himalayas, Herman *et al.* (2010) suggest a dip of 15° for a ramp that begins ∼70 km North of the MFT. More recently, Robert *et al.* (2011) have proposed models in which the MHT exhibits lateral variations in terms of geometry along the Himalayan arc.

In eastern Nepal, the Himalayan–Nepal–Tibet seismic experiment (HIMNT) reveals the deepening of the Moho beneath the range from ∼35 km under the MFT to ∼75 km beneath the IYS (Schulte-Pelkum *et al.* 2005). West of this profile along ∼85°E, the same trend is imaged by the Hi-CLIMB project (Himalayan–Tibetan Continental Lithosphere during Mountain Building) with RFs calculations. As this experiment runs farther north than HIMNT, it covers the underthrust and flattened Indian lower crust extending from the IYS until near the Banggong–Nujiang Suture (Nabelek *et al.* 2009). The top of the Indian lower crust (∼15 km thick) is well imaged especially beneath southern Tibet where it is interpreted to be eclogitized (Wittlinger *et al.* 2009). Bouguer anomaly profiles across the range show a variation of about −500 mGal from India to southern Tibet and confirm the northward thickening of the crust (Karner & Watts 1983; Lyon-Caen & Molnar 1985; Jin *et al.* 1996). Beneath the range, the gravity data are no longer consistent with Airy isostasy suggesting that the weight of the Himalayas is supported by the strength of the underthrusting India Plate (Cattin *et al.* 2001). By combining these data with thermomechanical modelling, Hetényi *et al.* (2006) have shown that the Effective Elastic Thickness (EET) decreases from 60–80 km in India to 20–30 km beneath Tibet where the Himalayas are mostly supported by the Indian lithospheric mantle. Based on forward gravity modelling and petrological models, Hetényi *et al.* (2007) suggest that the Indian lower crust has to be eclogitized in order to explain both seismological and gravity data.

The gravity data also exhibit a kink associated with the density contrast of the Ganga Basin, with its depth mainly control by the flexural subsidence of the India Plate (Lyon-Caen & Molnar 1985). South of Nepal, the foreland basin has a variable width with a mean extent of about 200 km and reaches a maximum depth of 6 km in the Gandak depression. The basement of the Ganga Basin is affected by inherited structures showing a succession of spurs and depressions. Three depressions are separated by two highs in the basement: from west to east, the Sarda depression, the Faizabad ridge, the Gandak depression, the Munghyr Saharsa ridge and the Purnea Basin. Each ridge is connected with an Archean massif, which crops out south of the basin, respectively, the Bundelkhand massif and the Satpura massif (Raiverman *et al.* 1983; Gahalaut & Kundu 2012).

3 GRAVITY AND SEISMOLOGICAL DATA

3.1 Available gravity data set

For this study, we merge three sources of existing gravity data (Fig. 1). In India, Bouguer anomalies are provided by the Bureau Gravimétrique International (BGI—http://bgi.omp.obs-mip.fr/). The data are tied to IGSN 71 reference with a reduction density of 2670 kg m^{-3} but do not include terrain correction. North of Nepal, gravity anomalies are taken from the 5 × 5 arcmin gridded Bouguer anomaly map (Sun 1989) resampled at the measurement locations. Those Bouguer anomalies were also calculated using a reduction density of 2670 kg m^{-3} and include terrain correction. In Nepal, gravity data are available from joint French–Nepali surveys along three profiles perpendicular to the Himalayan arc (Cattin *et al.* 2001; Martelet *et al.* 2001). The corresponding Bouguer anomalies computed with terrain correction and a reduction density of 2670 kg m^{-3} have an accuracy ranging from 0.5 to 5 mGal. Even though all these data sets are relative, they are consistent with the BGI reference (Hetényi *et al.* 2007). Their compilation allows us to obtain a gravity map from India to Tibet, but with a major data coverage gap in Nepal west of Kathmandu.

3.2 New gravity data, acquisition and processing

To complete this available data set and fill the existing data coverage gap in central Nepal, three Scintrex CG5 relative gravimeters, previously intercalibrated, were used to obtain 80 new gravity observations. Due to survey loops needed to correct instrumental drift, 120 measurements are carried out along two profiles, a 300-km-long parallel to the strike of the range from Kathmandu to Ameliya and a 150-km-long arc-perpendicular at the longitude of Pokhara extending from Siddharthanagar in the South to Jomosom in the

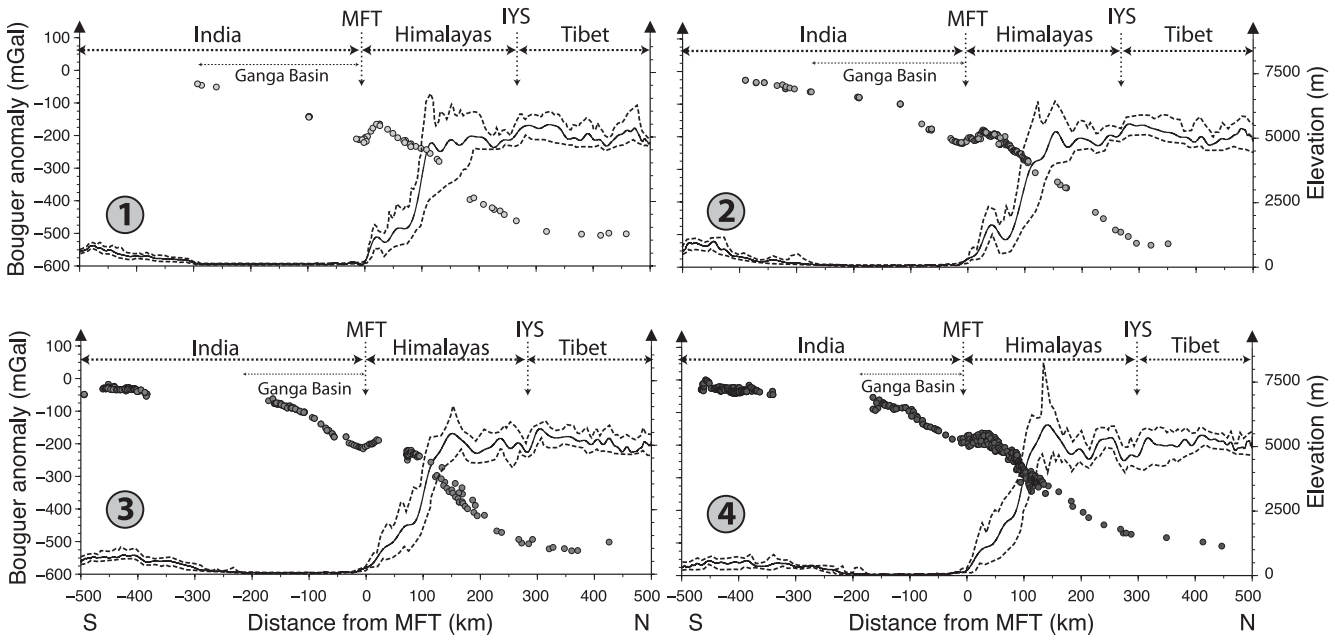

Figure 2. Bouguer anomaly along the four 1000-km-long N16°E profiles (see Fig. 1 for location of the profiles). All the data within a 25-km-wide swath on both sides of the profiles were considered and error bars lie within the circles. The profiles are centred at the surface location of the MFT. Location of MFT and IYS as well as extension of the Ganga Basin are also shown. The area between the two dashed lines represent the topography on a 25-km-wide swath for each profile from SRTM data with the black line corresponding to the average.

North (Fig. 1). For each site, at least five gravity measurements of 90 s and 15 min of GPS observations with dual-frequency geodetic receivers are made. The accurate locations of our measurements are obtained by double difference processing with Trimble Geomatic Office and the cGPS (continuous Global Positioning System) stations operated by the CEA (Commissariat à l'Énergie Atomique)/LDG (Laboratoire de Détection et de Géophysique) and the National Seismological Center in Kathmandu. We obtain a vertical height accuracy of less than 60 cm for all data points. The EGM08 geoid model is then used to convert ellipsoidal heights to elevations. Gravity measurements are corrected for ocean and earth tides using FES2004 model (Lyard *et al.* 2006) and ETERNA package (Wenzel 1996), respectively. We also correct for the linear drift of the gravimeter after daily loops. The free air anomaly is computed using the GRS67 ellipsoid and we estimate its accuracy to be of the order of 0.15 mGal. The complete Bouguer anomaly is calculated with a reduction density of 2670 kg m^{-3}. Terrain corrections are computed using TCQ package (Hwang *et al.* 2003) with SRTM digital elevation model for an inner zone of 20 km and an outer zone of 200 km. The accuracy of the final complete Bouguer anomaly depends on the terrain roughness and ranges between 0.15 and 0.60 mGal, knowing that the main source of error is the accuracy of the vertical position.

3.3 Consistency of data sets

In order to use the gravity data set obtained in this study together with the existing Bouguer anomaly data set, they have to be consistent in terms of reference and corrections. The same reduction density is used to calculate the Bouguer anomalies of both data sets. The free air anomalies for the new points are computed with the GRS67 instead of GRS80 to be consistent with the existing data set. All the new measurements are tied to absolute gravity base-stations in Kathmandu, Simra, Siddharthanagar and Tansen. These points have a measured accuracy of less than 0.01 mGal and are defined in the IGSN71 Network as the data provided by BGI. Furthermore, to check the consistency with previous studies, we compare the new measurements with the existing ones at close location. Inset of Fig. 1 shows a very good agreement between the data sets, with a discrepancy of only a few mGal.

3.4 Bouguer anomaly profiles

Our new measurements together with the available Bouguer anomalies allow constructing four profiles, 1000 km long each, perpendicular to the strike of the orogen (oriented N16°E) and centred on the MFT (Fig. 2). The profiles cover a 350-km-wide area in central and eastern Nepal between the Pokhara valley and the Arun river. Along each profile, the Bouguer anomaly decreases between −25 mGal to the south and −525 mGal to the north. The ∼500 mGal decrease occurs in about 600 km from south of the Ganga Basin above the India Plate to the Indus–Yarlungo Suture Zone on the Tibetan Plateau. Based on the shape of the Bouguer anomaly variations, these profiles can be divided into three distinct zones:

(i) The India section, from −500 km to 0 km distance, exhibits a convex curve with a decrease of ∼200 mGal. The first part of this section, which is nearly flat with a very low gradient corresponds to the signature of the India Plate and the beginning of its flexure. The second part, with a steeper gradient, can be related to the additional effect of the Ganga Basin where low-density sediments have been accumulated.

(ii) The Tibetan Plateau section, from 300 km distance onwards, begins close to the location of the IYS Zone and shows a flattening of the Bouguer anomaly at a value of ∼ −525 mGal.

(iii) In between these two sections lies the Himalaya section. It begins near the MFT with a local minimum corresponding to the maximum thickness of sediments accumulated in the Ganga Basin, then the Bouguer anomaly increases by ∼50 mGal on a distance that varies somewhat between profiles. After reaching a local maximum, near the MBT, the Bouguer anomaly decreases to reach the

aforementioned plateau at the beginning of the Tibetan section. Despite the average gradient being similar in all the profiles, we observe minor variations. For example, profile 1 exhibits two different gradients in this zone.

By comparing these four profiles we observe that the long-wavelength anomaly, which presumably reflects deepening of the Moho, is quite similar on all four profiles. In contrast, Fig. 2 shows that lateral variations in the Bouguer anomaly signal exist at shorter wavelengths, especially in the Ganga Basin and in the Himalaya section.

3.5 RF profiles

The Moho is the main interface within the lithosphere that reflects the geometry of the flexure and mainly controls the location of density contrasts. To complement the constraints on the shape of the plate flexure given by gravity anomalies, we search for available seismological profiles showing the geometry of the Moho. Among passive seismological methods, the Moho is best imaged using RFs: teleseismic *P* waves that convert to *S* waves beneath the observing station. The delay of the converted *S* wave with respect to the direct *P* wave contains information on the depth of the Moho and the average velocity structure of the crust (Langston 1977).

In Nepal clear images of the Moho are readily available from migrated RF images for profile 2 (Hi-CLIMB experiment, main array) as well as for the region of profiles 3 and 4 (HIMNT experiment; Fig. 1). For profile 1 associated with our new gravity data, we process the seismological data from 15 stations of the Hi-CLIMB experiment's Nepal–Pokhara (NP) line (Fig. 1), deployed along the road along which the gravity measurements were made. These stations were operating between 4 and 5 months, and registered teleseismic waveforms from a total of 161 earthquakes of $M5.5$ or above. The collected data were passed through a quality control procedure to yield 727 high-quality traces. RFs were computed using iterative deconvolution with a maximum frequency of the signal at 1 Hz. These RFs were then migrated from time to depth using the 2-D-velocity model of the Hi-CLIMB main array including correction for topography. Complete information on the Hi-CLIMB experiment as well as the RF processing is described in Hetényi (2007) and Nabelek *et al.* (2009).

The final RF image for profile 1 is shown in Fig. 3. Despite some noise in the Himalayan foothills, already observed along the main array, the Moho of the India Plate can be followed along ∼150 km distance and can be identified with an uncertainty of ∼5 km. The image shows a flat Moho at about 35 km depth in the south, which starts

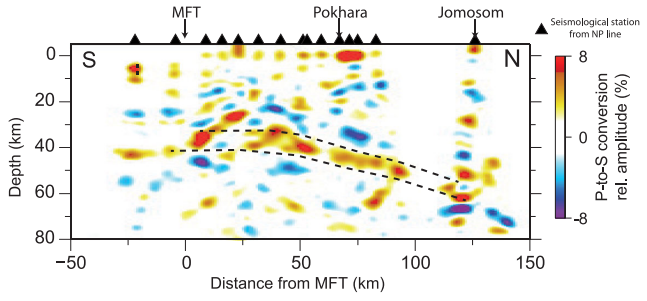

Figure 3. Migrated receiver function image along profile 1 (see Fig. 1 for location) using 15 stations of the Hi-CLIMB experiment's Nepal–Pokhara line. The Moho appears clearly in warm colours as a positive amplitude conversion of *P*- to *S* waves, and can be followed along the profile between the dashed lines. See text for more details.

to dip down north of the MFT at an angle of ∼12° to reach ∼60 km depth beneath the northernmost station. In comparison to the RF images of profiles 2, 3 and 4, this profile is shorter but shows a similar trend: a flat Moho turning to a ramp at a similar angle. Compared to other profiles, the flat-to-ramp transition here is more abrupt (Fig. 6), but considering the error bars the difference is not significant.

With the processing of seismological data from the Hi-CLIMB experiment's NP line, the flexural shape of the underthrusting India Plate within the entire study area can be constrained both by gravity and seismological data.

4 THERMOMECHANICAL MODELLING

Deviations of the gravity field across the Ganga Basin and the Himalayas from local Airy isostasy, are commonly interpreted to result from the elastic support provided by the flexed Indian Plate (Cattin *et al.* 2001). The flexural shape of the lithosphere depends on its composition, its thermal structure and the thickness of the composing layers. Across the Himalayas the changes of these parameters can be simulated by varying the thickness of an elastic plate overlying an inviscid fluid and loaded by masses above (e.g. Karner & Watts 1983; Lyon-Caen & Molnar 1985; Jordan & Watts 2005). In such an approach the dependency of deformation on local temperature and pressure as well as the relative effect of the crust and mantle cannot be dealt with. Thus, following Cattin *et al.* (2001) and Hetényi *et al.* (2006) we use a more comprehensive approach that accounts for the mechanical layering of the lithosphere, the non-Newtonian rheology of rocks and their dependency on temperature and pressure. We use a 2-D finite element model, ADELI (Hassani *et al.* 1997), that was modified to incorporate both temporal and spatial variations of the loading.

4.1 Rheology and thermal structure of the India lithosphere

In our model the India Plate is composed of three bodies: upper crust, lower crust and lithospheric mantle (Fig. 4). These three layers are deformed in an elastic, brittle or ductile way depending on the local deviatoric stresses, pressure and temperature. The elasticity is expressed by Hooke's law,

$$\varepsilon_{ij} = \frac{1+\nu}{E}\sigma_{ij} - \frac{\nu}{E}\mathrm{tr}\,(\sigma)\,\delta_{ij}, \tag{1}$$

with ε the strain tensor, σ the stress tensor, E the Young's modulus and ν the Poisson's ratio. The non-Newtonian viscous behaviour, dependent on temperature T, is controlled by the following relationship between differential stress and strain rate $\dot{\varepsilon}$:

$$\dot{\varepsilon} = \gamma_0\,(\sigma_1 - \sigma_3)^n\, e^{\frac{E_a}{RT}}, \tag{2}$$

where γ_0 is the standard fluidity, n the power-law exponent, E_a the activation energy and $R = 8.314\,\mathrm{J\,mol^{-1}\,K^{-1}}$ the universal gas constant. σ_1 and σ_3 are the maximum and minimum principal stress, respectively. The limit between the viscoelastic and the plastic domains is defined by Drucker–Prager failure criterion, according to

$$\frac{1}{2}\,(\sigma_1 - \sigma_3) = \left(c\,(\cot\phi) + \frac{1}{2}\,(\sigma_1 + \sigma_3)\right)\sin\phi, \tag{3}$$

with ϕ and c the internal friction angle and the cohesion, respectively. The laboratory-derived material properties are used under the assumption that they can be extrapolated to geological conditions (Table 1).

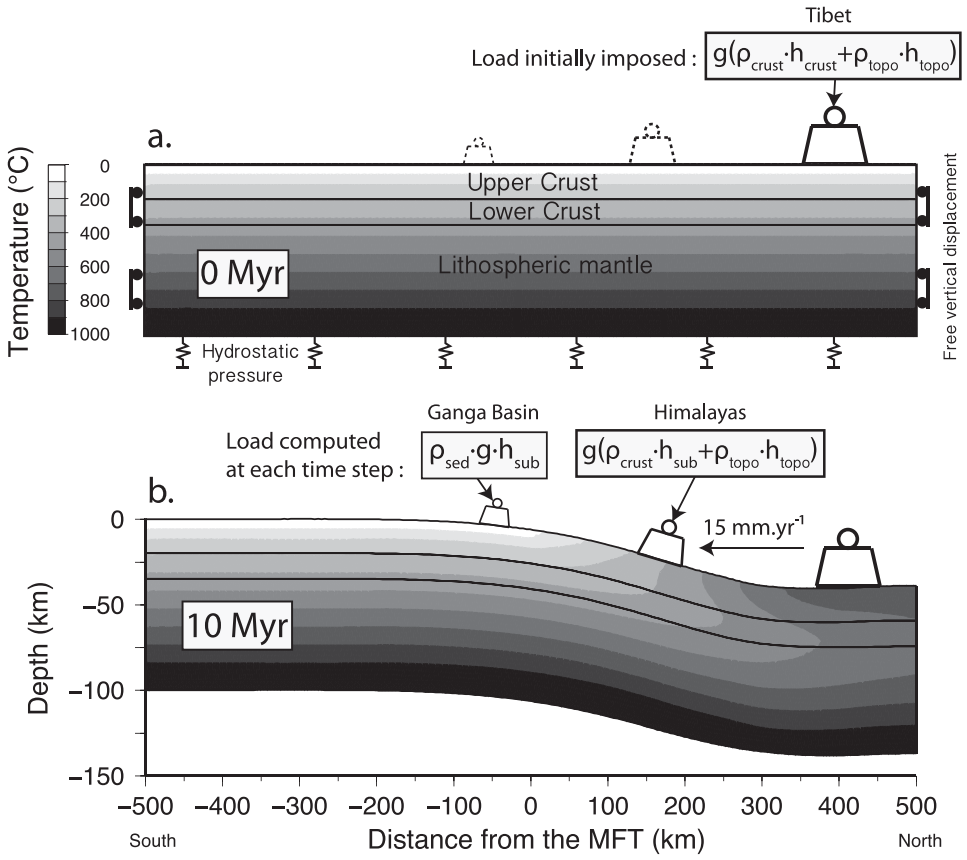

Figure 4. (a) Geometry, boundary conditions and temperature of the initial model used for the thermomechanical modelling with ADELI (Hassani *et al.* 1997). The Indian lithosphere is progressively bent down by the vertical load applied on its top. The loading moves southwards at a rate of 15 mm yr^{-1} and corresponds to the increasing weight of the sediments in the foreland, Himalayas and the Tibetan Plateau. The model is subject to gravity and is sustained by hydrostatic pressure at its base. Free vertical displacements are allowed at both sides of the model. The three layers considered have different rheologies (described in Table 1). (b) Geometry and temperature field of the model after 10 Myr.

Table 1. Rheological parameters used for the thermomechanical modelling. ρ, density; E, Young's modulus; ν, Poisson's ratio; c, cohesion; ϕ, internal friction angle; γ_0, power-law strain rate; n, power-law exponent and E_a, power-law activation energy.

	Upper crust (Quartz)	Lower crust (Diabase)	Upper mantle (Olivine)
ρ (kg m^{-3})	2800	2900	3270
E (GPa)	100	100	100
ν	0.25	0.25	0.25
c (MPa)	10	10	10
ϕ	30°	30°	30°
γ_0 (Pa^{-n} s^{-1})	6.31×10^{-25}	6.31×10^{-20}	7×10^{-14}
n	2.90	3.05	3.00
E_a (kJ mol^{-1})	149	276	510

The thermal structure of our model is computed from an analytical approach based on the 1-D approximation of Royden (1993). In this calculation [following Cattin *et al.* (2001)], the temperature is mainly controlled by the geometry of the India Plate. The thermal structure in the initial time step and in the final model are shown in Fig. 4. This thermal field is consistent with the well-constrained model presented by Bollinger *et al.* (2006) based on numerous field observations across the Himalayan range in central Nepal.

4.2 Geometry and boundary conditions

To simulate the flexure of India, we use a 1000-km-long flat plate centred on the MFT (Fig. 4). As an initial condition, we consider 9000 triangular elements to compose the three layers. The crust is 35 km thick (Kumar *et al.* 2001) and its density contrast with the lithospheric mantle is 370 kg m^{-3}. The model is submitted to gravitational force ($g = 9.81$ m s^{-2}), supported by hydrostatic pressure at its base with a vertical density profile taken from the PREM (Dziewonski & Anderson 1981).

To simulate the bending of the plate, both vertical sides of the model allow for free vertical displacement and the top of the India Plate is loaded by the mass of the Himalayas and the Tibetan Plateau. Compared to Cattin *et al.* (2001) we have improved the model by applying a more realistic loading, which evolves during the numerical simulation. This vertical loading on top of the India Plate excludes shear forces and is calculated at each time step by adding the effect of surface load (topography) and subsurface loads (Tibetan crust and of the sediments accumulated in the foreland basin).

We calculate the topographic load by averaging the topography in the four studied profiles and we assume a mean density of 2670 kg m^{-3} above 0 m (Fig. 6a). For the crustal material above the India Plate, we use a constant Moho depth of 75 km beneath Tibet, where both HIMNT and Hi-CLIMB experiments (Schulte-Pelkum *et al.* 2005; Nabelek *et al.* 2009) reveal a flattening of the Moho at the latitude of the IYS (~300 km distance on our projected profile).

Thus, as we do not consider transfer of material between India and Tibet during the numerical simulation, the pressure applied north of the IYS is constant and equals to the load of an ∼45-km-thick Tibetan crust including topography.

From south of the IYS to the MFT, and for the foreland basin, the load depends on the geometry of the bent India Plate. It implies that the load ΔP is calculated, at each time step, depending on the northward deepening of the India Plate $h_{\rm sub}$ by

$$\Delta P = \rho \cdot g \cdot h_{\rm sub}, \tag{4}$$

where ρ is 2500 kg m^{-3} south of the MFT to reflect the lower density of sediments accumulated in the foreland basin and 2900 kg m^{-3} north of the MFT, an average for the whole Tibetan Crust.

This loading is applied during 10 Myr on the India Plate with a north-to-south movement corresponding to an underthrusting rate of 15 mm yr^{-1} (Cattin *et al.* 2001). These 10 Myr are divided in 4000 time steps in our experiment and correspond to the order of magnitude for the estimated time of the India Plate flexure. We then stop the evolution of the loading and obtain a nearly steady-state geometry, which we will consider hereafter.

The main limitation of the used thermomechanical model is that it is 2-D and that it neglects horizontal shortening. Moreover, we do not take into account the rheological behaviour of the eclogite layer in the India lower crust underneath Tibet because of a lack of reliable rheology data at this pressure–temperature range and technical limitations of the modelling tool. In the following we analyse profiles across the Ganga Basin, the Himalayas and southern Tibet, perpendicular to the main geological structures.

5 RESULTS

The effects of the thermal structure, the rheological parameters as well as the thickness and the density of the lithospheric layers are tested using a large amount of numerical experiments with various density contrast at the Moho, crustal and lithospheric thickness, Poisson's ratio, Young's modulus, viscous power-law parameters, temperature at the basis of the lithosphere and thermal conductivity.

Complexity of the modelling lies in the trade-off between parameters, which control the flexural rigidity. For instance an increase in the basal temperature gives a warmer thermal structure resulting in a smaller curvature which can be compensated by using stronger rheologies for the lithosphere. It results in the non-uniqueness of the solutions. Due to computation time, here we only test the effect of parameters separately.

Some of these parameters have only a small influence on the final geometry of our model such as the density or the thickness of the layers. Thereby, hereinafter we fix the density contrast at the Conrad discontinuity to 100 kg m^{-3} and at the Moho to 370 kg m^{-3} (Cattin *et al.* 2001), the crustal thickness to 35 km (Kumar *et al.* 2001) or the thickness of the lithosphere to 100 km (Kumar *et al.* 2007; Devi *et al.* 2011).

In contrast, the elastic parameters, the temperature field or the viscous rheology has a greater effect on the final geometry of the India Plate. Fig. 5 shows the results for the exploration of four parameters and their influence on calculated Bouguer anomaly and Moho geometry. To compare models with the data, we calculate a χ^2 misfit following this formula:

$$\chi^2 = \sum_{i=1}^{n}\left(\frac{G\text{data}_i - G\text{model}_i}{\sigma G_i}\right)^2 + \alpha \sum_{k=1}^{m}\left(\frac{M\text{data}_k - M\text{model}_k}{\sigma M_k}\right)^2, \tag{5}$$

where G and M correspond to gravity anomalies and geometry of the Moho, respectively. n and m, the number of data for gravity and RFs and σ their associated error. We use a coefficient, $\alpha = 20$, in order to balance the weights between gravity and RF misfits.

The basal temperature has a strong control on the flexural rigidity of the plate: higher temperatures lower the flexural rigidity. Our results also suggest that the Young's modulus has a first-order control on the final geometry below the threshold value of ∼80 GPa (Fig. 5).

Using various viscous rheologies proposed by Ranalli (1995), our results demonstrate that, compared to the mantle, the crustal rheology has a minor effect on the shape of the flexure. Furthermore our results suggest that compared to a dry mantle, a wet mantle leads to a smaller curvature.

In our preferred model, we use a basal temperature of 977 °C, an upper crustal heat production of 2.5 μW m^{-3} and a thermal conductivity of 2.5 W m^{-1} K^{-1}. The calculated surface heat flow from this thermal structure is about 60 mW m^{-2}, consistent with the measurements made in cratonic areas of northern India (Pandey & Agrawal 1999). We obtain the best fit with the parameters described in Table 1, which correspond to a weak upper crust, strong lower crust and strong mantle.

5.1 Consistency with seismological data

The Moho geometry of our best fit model is consistent with the constraints given by HIMNT and Hi-CLIMB project (Schulte-Pelkum *et al.* 2005; Nabelek *et al.* 2009) as well as with the new RFs profile obtained at the longitude of Pokhara (Fig. 6b). This model suggests a smoothly bent geometry for the Moho, which starts to bend down with a low angle at about −250 km distance in our profile. Its dipping angle gradually increases underneath the Ganga Basin to reach the steepest dip of 11° northwards beneath the High Himalaya. Then the Moho flattens at 300 km.

Between the onset of the flexure of the India Plate and the location of the MFT, the top of our model corresponds to the basement of the Ganga Basin. It is also in good agreement with the constraints on the depth of the basement from RFs (Hetényi *et al.* 2006), from a deep well (Sastri *et al.* 1971) and from a basement depth contour map of the Gangetic plains (Raiverman *et al.* 1983) showing a maximum depth of 6 km and a mean horizontal extent of ∼250 km.

More importantly our results suggest that a single lithosphere rheology type explains Moho depth constraints over the lateral distance of 350 km studied here. Minor lateral variations of Moho depth seen on RF constraints could not be explained by numerical models using homogeneous layer properties tested here, which likely points to small along-profile heterogeneities in physical properties. Nevertheless, the gross picture is satisfactory, although better seismological coverage could improve the set of constraints. Next we analyse gravity data to test the hypothesis of lateral similarity of India Plate strength from central to eastern Nepal.

5.2 Long-wavelength gravity data and EET of the India Plate

We use the final geometry of the modelled India Plate layers to calculate the synthetic Bouguer anomalies and compare them to the observations along the four gravity profiles. We assume the same density contrasts as in our thermomechanical model for the India Plate : 100 kg m^{-3} at the Conrad discontinuity and 370 kg m^{-3} at the Moho. For consistency between thermomechanical modelling and

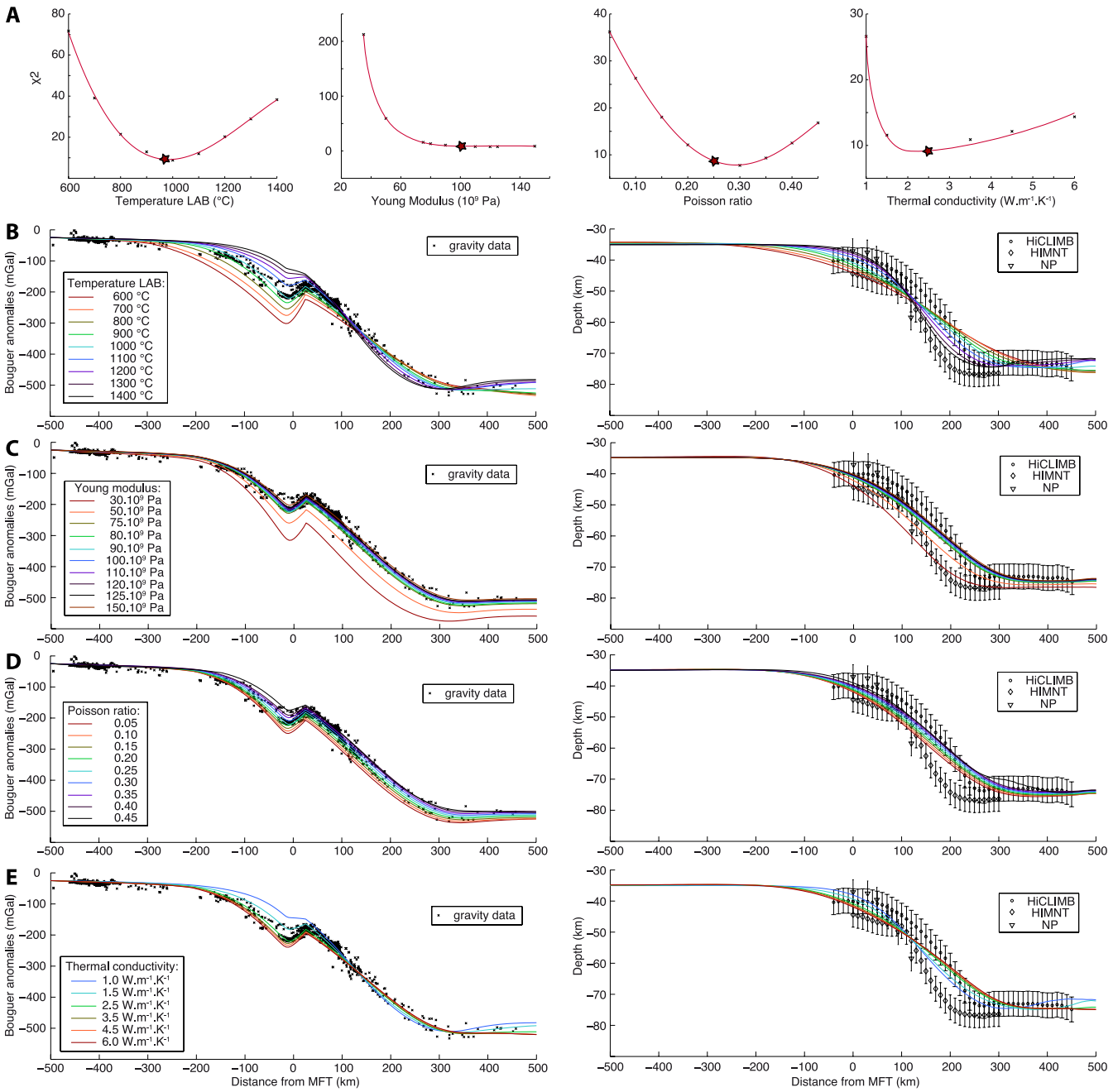

Figure 5. Effect of temperature at the lithosphere–astenosphere boundary (LAB), Young's modulus, Poisson's ratio and thermal conductivity. (a) χ^2 function of the different tested parameters. The red star corresponds to our preferred model. (b) Effect of the LAB temperature on our models. On the left-hand side, the coloured lines and crosses correspond to the calculated Bouguer anomaly and to the data, respectively. On the right-hand side are shown in colour the Moho geometries obtained in our models and in black the constrained from receiver function profiles. (c) Same as (b) for Young's modulus. (d) Same as (b) for Poisson's ratio. (e) Same as (b) for thermal conductivity.

gravity modelling, the density of the Tibetan crust and sediment in the foreland basin are the same than those used in the calculation of the load applied on top of the India Plate (Fig. 6b). The synthetic Bouguer anomalies are computed following the approach proposed by Won & Bevis (1987).

The calculated long-wavelength anomalies are in fairly good agreement with the gravity data except beneath the Tibetan Plateau, where they are lower than the observed data by ∼70 mGal (Fig. 6). Several studies argue in favour of the eclogitization of the Indian lower crust beneath Tibet (e.g. Henry *et al.* 1997; Schulte-Pelkum *et al.* 2005; Tiwari *et al.* 2006; Monsalve *et al.* 2008) and as proposed by Hetényi *et al.* (2007), eclogitization presumably occurs as it reaches its maximal depth, that is, at the location where we observe the misfit between calculated and observed gravity data. The fit is improved by increasing the density of the Indian lower crust beneath Tibet for $\Delta\rho = 150\,\mathrm{kg\,m^{-3}}$ with respect to the Moho. The final model gives consistent results with the gravity data on a large scale along all four profiles, confirming the seismological result of lateral similarity of the India Plate between the longitude of Pokhara and the Arun river (Fig. 6).

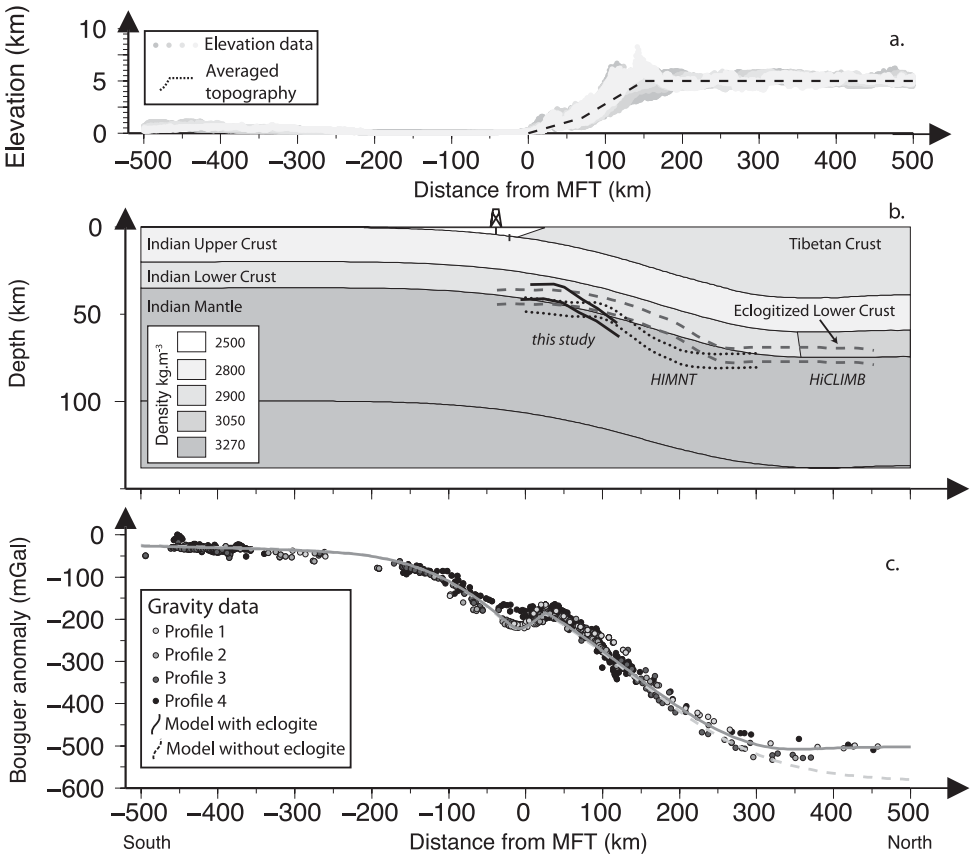

Figure 6. Topography, preferred flexural model and the associated Bouguer anomaly compared with observed data along the four profiles. (a) Topography on a 25-km-wide swath for the four profiles. Dashed black line corresponds to the averaged topography used in the calculation of the subsurface load. (b) Final geometry of the thermomechanical model after 10 Myr. To explain the long-wavelength anomaly, we increase the density of the Indian lower crust that is underthrusting Tibet where eclogitization occurs. Different geometrical constraints from published receiver functions at different profiles as well as from the depth constraint of the Raxaul deep well are also shown. (c) Circles represent the Bouguer anomaly along the four profiles (see Fig. 1 for location of the profiles). The thick black line corresponds to the calculated gravity anomaly associated with the flexural model below, the dashed one correspond to the model without eclogite.

The estimate of the flexural rigidity of the India Plate remains highly variable (e.g. Karner & Watts 1983; Lyon-Caen & Molnar 1983; Burov & Watts 2006; Hetényi *et al.* 2006; Chamoli *et al.* 2011; Hammer *et al.* 2013). This variability can be related to the used approach (forward modelling versus spectral methods), but it can also reflect some real lateral variations. Taking advantage of our new gravity and seismological information we address the question of the strength of the India lithosphere, that is, its flexural rigidity, in central and eastern Nepal. To allow some comparison with thin elastic plate models, our model can be interpreted in terms of the EET. The depth-varying rheology leads to the development of weak layers within the lithosphere and decoupling (Fig. 7), responsible for variations of the mechanical rigidity of the Indian lithosphere. For a plate decoupled into n layers, the equivalent EET of the plate is given by (e.g. Burov & Diament 1992):

$$\mathrm{EET} = \left(\sum_{i=1}^{n} h_i^3 \right)^{1/3}, \tag{6}$$

where h_i is the thickness of the elastic core for the i-th layer. The deformation is considered elastic when the relaxation time τ of the material is twice as long as the time of the numerical experiment with:

$$\tau = \frac{\nu}{E}, \tag{7}$$

where ν is the effective viscosity and E the Young's modulus. Here we assume that a region will be elastic when the effective viscosity is larger than $\sim 2 \times 10^{25}$ Pa s for a modelled deformation age of 10 Myr. The calculated effective viscosity from our thermomechanical model is thus used to assess the EET associated to a layered India Plate with an ∼35-km-thick crust and a Conrad discontinuity at 20 km depth.

Our results suggest a flexural rigidity decrease of the India Plate from ∼75 km in the south of the profile at 24N° to ∼25 km beneath the Tibetan Plateau at 32N° (Fig. 7). This decrease has been already suggested by Karner & Watts (1983) by implicitly breaking the elastic plate at the suture. The EET of the upper and lower crust decreases beneath the Ganga Basin and vanishes beneath the Himalayas, 100 km North of the MFT, at about 27.5N°. The EET of the mantle decreases slowly along the profile from a value of 40 to 25 km. It suggests that the mantle rheology is the prime control on India Plate flexure (Karner *et al.* 1983). Coupling between crust and mantle exists until −250/−350 km distance. North of ∼25N°, the three layers are decoupled. This results in a non-linear EET

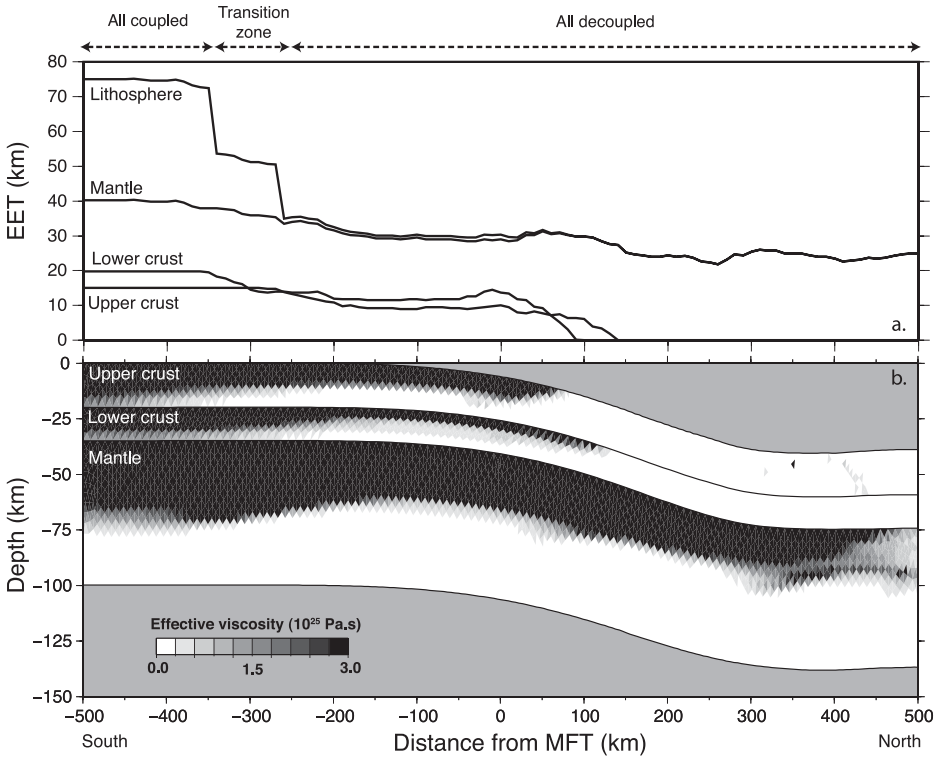

Figure 7. Effective viscosity of the preferred model and the corresponding Effective Elastic Thickness (EET). (a) EET for each layer and for the whole lithosphere. Depending on the coupling of the layers, EET is ∼75 km south of our profile and decreases northwards because of crustal thickening, temperature increase and decoupling to reach ∼25 km to the north. (b) Effective viscosity plotted for each layer composing the India Plate. Dark areas correspond to the strong and elastic part of the lithosphere whereas light one represents the weak and ductile part.

decrease along the profile: in the southern part all layers are coupled and the India Plate has an EET of ∼75 km. Further north the successive decoupling of the base of the upper and lower crust leads to an ∼100-km-long transition zone where the EET drops to ∼50 km. All the layers are decoupled at about −250 km distance where the EET drops to ∼35 km, north of which it decreases slowly to reach ∼25 km beneath Tibet.

5.3 Lateral variations of short-wavelength gravity anomalies and subsurface structures

The geometry of the India Plate and its associated strength presented in Figs 6 and 7 account for the regional trend of the gravity data along the four profiles. However, small differences between these profiles and our forward modelling exists, especially in the Ganga Basin and in the Himalayan section (Fig. 8a). In this figure, we removed the gravity effect of the low-density sediments in the Ganga Basin from our model to enhance its variability in the residuals of the four profiles. We can note two main features in these residuals, a gravity low south of the MFT with a maximum value of about −100 mGal and a gravity high of 50 mGal observed at ∼125 km north from the MFT. The gravity low south of the MFT corresponds to the effect of accumulated sediments in the Ganga Basin (Lyon-Caen & Molnar 1983). It exhibits a decrease both in width and amplitude from west to east. This can be easily explained by the rough topography of the basement and especially by the presence of the Munghyr Saharsa ridge near by the easternmost profile 4. Regarding the gravity high, its location lies at the TSS and should related to the thick sedimentary cover. Here, part of the signal in the Bouguer anomaly could be linked with a overestimated reduction density compared to the rest of the Himalayas.

Short-wavelength gravity data along profile 2 have already been interpreted in terms of density contrast of foreland sediments, of Lesser Himalayan metasediments and of Palung granites (Cattin *et al.* 2001). Here we focus on profile 1 that corresponds to our new gravity data to show that a simple gravity modelling of subsurface structures fit the two areas of short-wavelength misfit. For the Ganga Basin, as already shown, we assume a density contrast of $-420\,\mathrm{kg\,m^{-3}}$ with respect to the rest of the model and a simplified geometry: a straight south-dipping line starting from the surface location of MBT to the top of the India Plate at depth. The TSS is assumed to extend to 8 km depth (Zhang & Klemperer 2010) with a low angle northward dip of the South Tibetan Detachment (STD; Searle 2010) and a density contrast of $-100\,\mathrm{kg\,m^{-3}}$, corresponding to the value used by Tiwari *et al.* (2006) considering the density of $2670\,\mathrm{kg\,m^{-3}}$ for the rest of our model. The observed and calculated Bouguer anomalies are in very good agreement, with a maximum and an average difference of 10 mGal and 2 mGal, respectively (Fig. 8b). It thus turns out that the small lateral gravity variations that remain in our four profiles once the flexural support of the range is taken into account, are linked to variations of geometry and density of subsurface structures.

6 DISCUSSION

The new thermomechanical modelling carried out in this study, together with a new set of gravity and seismological data, allows us to reestimate the EET of the India Plate in central and eastern Nepal. Regarding the similarity in the long-wavelength anomalies along the four study profiles, it appears that there are no major lateral variations of the India Plate strength in this ∼350-km-wide

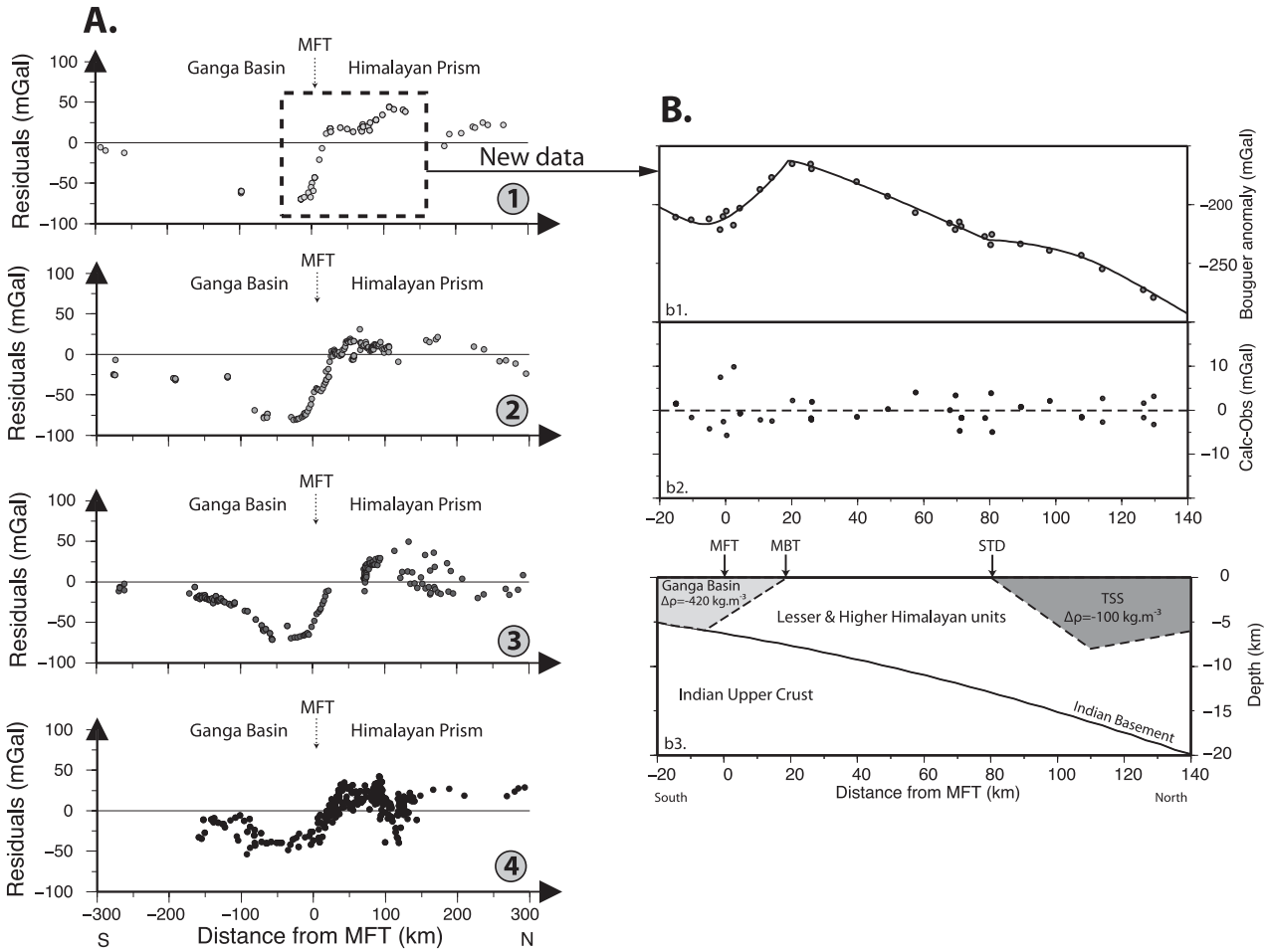

Figure 8. (a) Bouguer anomaly residuals for the four studied profiles calculated by subtracting the synthetic Bouguer anomaly associated to the thermomechanical model (without the gravity effect of the Ganga Basin) from the observed data. (b) Flexural model and associated Bouguer anomaly centred on the new data set (profile 1) to adjust the residuals at short wavelength: (b1) calculated (black line) and observed (circles) Bouguer anomalies; (b2) calculated minus observed gravity anomalies; (b3) density model with flexural geometry of the final model. The Ganga Basin is ascribed a density contrast of $-420\,\mathrm{kg\,m^{-3}}$, that is, $2250\,\mathrm{kg\,m^{-3}}$ considering an upper crustal density of $2670\,\mathrm{kg\,m^{-3}}$. The Tethyan Sedimentary Series is assumed to extend to 8 km depth (Zhang & Klemperer 2010) with a low angle northward dip of the STD (Searle 2010) and a density contrast of $-100\,\mathrm{kg\,m^{-3}}$ in agreement with the $2570\,\mathrm{kg\,m^{-3}}$ found by Tiwari *et al.* (2006).

area. The obtained EET profile is in agreement with the result of Hetényi *et al.* (2006) along a profile near Kathmandu. Our result is also consistent with the analytical solutions for the flexure of an elastic plate found by Lyon-Caen & Molnar (1983), Karner & Watts (1983), Jin *et al.* (1996) and Burov & Watts (2006). Jordan & Watts (2005) suggest variations in elastic thickness along strike of the Himalaya East of 87°E, our results are in agreement with their findings for the eentral Himalayas (western Nepal), which suggests the India Plate mechanical behaviour is similar all along Nepal. They also predict a northward decrease of the EET from ∼100 km in central India to ∼25 km beneath Tibet, also in agreement with our findings. In contrast, McKenzie & Fairhead (1997) and Jackson (2002) suggest an EET of ∼40 km south of the MFT, which is lower than our estimate. However a detailed analysis of their results suggests that the minimum value of EET from their misfit function is poorly constrained.

Even with the simplified geometry used for the northern end of the Ganga Basin, the short-wavelength anomaly analysis presented in Fig. 8(b) fits the observed data well. Such a modelling has already been performed along the Kathmandu profile by Hetényi *et al.* (2006) with the same density of sediments. A detailed forward gravity modelling has been realized by Cattin *et al.* (2001) along profile 2. They model the Ganga Basin with a northward dipping end with addition to the LH units but they do not include the TSS even if it lies all along the study area (Zhang & Klemperer 2010; Zhang *et al.* 2012). The explanation is that the STD is further north in profile 2 than in profile 1 and that there are no data at this location on profile 2. Regarding the gravity low associated to the Ganga Basin in the four profiles (Fig. 8), we can observe that its width decreases to the east, which is consistent with the isocontour map of the depth of the Ganga Basin (Raiverman *et al.* 1983; Gahalaut & Kundu 2012). Finally, the low in profile 4 is not as regular as in the other profiles which can be associated to the highly fractured basement at this location due to the basement high corresponding to the northern prolongation of the Satpura massif.

7 CONCLUSION

Using both geological and geophysical information as well as new gravity and seismological data sets we have addressed the question of lateral variations in the India Plate strength across the Himalayas

over central and eastern Nepal. Our new measurements and the available Bouguer anomalies allow obtaining four profiles, each 1000 km long, perpendicular to the strike of the orogen (oriented N16°E) and centred on the MFT. These profiles cover a 350-km-wide area in central and eastern Nepal between the Pokhara valley and the Arun river. Following Cattin *et al.* (2001) and Hetényi *et al.* (2006) we carry out thermomechanical modelling to interpret jointly these data in terms of flexural rigidity of the Indian lithosphere and crustal structures. Compared to these two previous studies the numerical modelling is improved by considering a more realistic vertical loading including spatial and temporal variations.

Our model fits both seismological and gravity data suggesting that these geophysical observations are compatible with the assumed material properties of crustal and mantle rocks. Our main result is that in the study area no major lateral variations of the strength of the India Plate are needed to fit the seismological constraints and gravity anomalies. This suggests that a homogeneous India Plate rheology with a strong mantle acts in the India–Eurasia collision in central and eastern Nepal. This finding is in agreement with the recent result obtained by Grandin *et al.* (2012) showing no variation in the interseismic loading between the front of the Annapurna mountain range (near Pokhara) and the Kathmandu valley. This is important in terms of seismic hazard assessment, because it promotes lateral continuity of the state of stress along an ∼350-km-wide zone that may control the seismological potential of this area.

The long-wavelength variation of the gravity anomaly in the four study profiles is the same. Our result confirms that the main trend of the gravity profile reflects the deepening of the Moho from 35 to 75 km and a (partially) eclogitized Indian lower crust beneath Tibet (Hetényi *et al.* 2007). Our model also predicts a northward decrease of the EET of the India Plate with three successive stages, with an EET of 75, 50 and 35–25 km, respectively, associated to an Indian lithosphere that is totally coupled south of the foreland, partially coupled in the foreland and totally decoupled beneath Tibet. At shorter wavelengths, the new data set can be explained by simply adding density contrasts corresponding to the Ganga Basin and to the Tethyan Sedimentary Sequence. The lateral variations in the gravity low attributed to the Ganga Basin reflect along-strike variations of basement depth.

The EET of the India Plate inferred from Bouguer anomaly profiles acquired in Sikkim (Tiwari *et al.* 2006), in Northwest Himalaya (Chamoli *et al.* 2011), as well as in Bhutan (Hammer *et al.* 2013) seem to be different from those obtained in Nepal. Further geophysical observations along missing portions of the Himalayan arc (western Nepal, northeastern India) are thus now needed to constrain the lateral variations in three dimensions.

ACKNOWLEDGEMENTS

This work was supported by grants from INSU-ALEAS and CNES-TOSCA. People from the Department of Mines and Geology as well as the drivers are thanked for their help in the field survey. Most of the figures of this paper were prepared using the Generic Mapping Tools software (Wessel & Smith 1995). We finally thank three anonymous reviewers for their constructive comments on the paper.

REFERENCES

Ader, T. *et al.*, 2012. Convergence rate across the Nepal Himalaya and interseismic coupling on the Main Himalayan Thrust: implications for seismic hazard, *J. geophys. Res,* **117,** B04403, doi:10.1029/2011JB009071.

Alsdorf, D., Brown, L., Nelson, K.D., Makovsky, Y., Klemperer, S. & Zhao, W.J., 1998. Crustal deformation of the Lhasa terrane, Tibet plateau from Project INDEPTH deep seismic reflection profiles, *Tectonics,* **17**(4), 501–519.

Avouac, J.P., Bollinger, L., Lave, J., Cattin, R. & Flouzat, M., 2001. Seismic cycle in the Himalayas, *C. R. L'Academie Des Sci. Serie IIA,* **333**(9), 513–529.

Bilham, R. *et al.*, 1997. GPS measurements of present-day convergence across the Nepal Himalaya, *Nature,* **386**(6620), 61–64.

Bollinger, L., Henry, P. & Avouac, J., 2006. Mountain building in the Nepal Himalaya: thermal and kinematic model, *Earth planet. Sci. Lett.,* **244** (1–2), 58–71.

Brown, L.D. *et al.*, 1996. Bright spots, structure, and magmatism in southern Tibet from INDEPTH seismic reflection profiling, *Science,* **274**(5293), 1688–1690.

Burchfield, B., Zhiliang, C., Hodges, K., Yuping, L., Royden, L., Changrong, D. & Jiene, X., 1992. The South Tibetan Detachment System, Himalayan orogen: extension contemporaneous with and parallel to shortening in a collisional mountain belt, *Geol. Soc. Am. Spec. Pap.,* **269,** 1–41.

Burov, E. & Diament, M., 1992. Flexure of the continental lithosphere with multilayered rheology, *Geophys. J. Int.,* **109,** 449–468.

Burov, E.B. & Watts, A.B., 2006. The long-term strength of continental lithosphere: 'jelly sandwich' or 'crème brûlée'? *GSA Today,* **16**(1), 4–10.

Cattin, R. & Avouac, J.P., 2000. Modeling mountain building and the seismic cycle in the Himalaya of Nepal, *J. geophys. Res.,* **105**(B6), 13 389–13 407.

Cattin, R., Martelet, G., Henry, P., Avouac, J.P., Diament, M. & Shakya, T.R., 2001. Gravity anomalies, crustal structure and thermo-mechanical support of the Himalaya of Central Nepal, *Geophys. J. Int.,* **147**(2), 381–392.

Chamoli, A., Pandey, A.K., Dimri, P. & Banerjee, P., 2011. Crustal configuration of the Northwest Himalaya based on modeling of gravity data, *Pure appl. Geophys.,* **168,** 827–844.

DeCelles, P.G., Robinson, D.M., Quade, J., Ojha, T.P., Garzione, C.N., Copeland, P. & Upreti, B.N., 2001. Stratigraphy, structure, and tectonic evolution of the Himalayan fold-thrust belt in western Nepal, *Tectonics,* **20**(4), 487–509.

Devi, E.U., Kumar, P. & Kumar, M.R., 2011. Imaging the indian lithosphere beneath the eastern Himalayan region, *Geophys. J. Int.,* **187**(2), 631–641.

Duncan, C., Masek, J. & Fielding, E., 2003. How steep are the Himalaya? Characteristics and implications of along-strike topographic variations, *Geology,* **31**(1), 75–78.

Dziewonski, A. & Anderson, D., 1981. Preliminary reference Earth model, *Phys. Earth planet. Inter.,* **25**(4), 297–356.

Gahalaut, V. & Kundu, B., 2012. Possible influence of subducting ridges on the Himalayan arc and on the ruptures of great and major Himalayan earthquakes, *Gondwana Res.,* **21**(4), 1080–1088.

Gansser, A., 1964. *Geology of the Himalayas,* Wiley.

Grandin, R., Doin, M.-P., Bollinger, L., Pinel-Puysségur, B., Ducret, G., Jolivet, R. & Sapkota, S., 2012. Long-term growth of the Himalaya inferred from interseismic InSAR measurement, *Geology,* **40**(12), 1–4.

Hammer, P. *et al.*, 2013. Flexure of the India plate underneath the Bhutan Himalaya, *Geophys. Res. Lett.,* **40**(16), 4225–4230.

Hassani, R., Jongmans, D. & Chéry, J., 1997. Study of plate deformation and stress in subduction processes using two-dimensional numerical models, *J. geophys. Res.,* **102**(B8), 17 951–17 966.

Henry, P., Le Pichon, X. & Goffé, B., 1997. Kinematic, thermal and petrological model of the Himalayas: constraints related to metamorphism within the underthrust Indian crust and topographic elevation, *Tectonophysics,* **273**(1–2), 31–56.

Herman, F. *et al.*, 2010. Exhumation, crustal deformation, and thermal structure of the Nepal Himalaya derived from the inversion of thermochronological and thermobarometric data and modeling of the topography, *J. geophys. Res.,* **115,** B06407, doi:10.1029/2008JB006126.

Hetényi, G., 2007. Evolution of deformation of the Himalayan prism: from imaging to modelling, *PhD thesis,* École Normale Supérieure - Université Paris-Sud XI. [http://tel.archives-ouvertes.fr/tel-00194619/en/]

Hetényi, G., Cattin, R., Vergne, J. & Nabelek, J.L., 2006. The effective elastic thickness of the India Plate from receiver function imaging, gravity anomalies and thermomechanical modelling, *Geophys. J. Int.,* **167**(3), 1106–1118.

Hetényi, G., Cattin, R., Brunet, F., Bollinger, L., Vergne, J., Nabelek, J. & Diament, M., 2007. Density distribution of the India plate beneath the Tibetan plateau: geophysical and petrological constraints on the kinetics of lower-crustal eclogitization, *Earth planet. Sci. Lett.,* **264**(1–2), 226–244.

Hirn, A. *et al.*, 1984. Crustal structure and variability of the Himalayan border of Tibet, *Nature,* **307**(5946), 23–25.

Hwang, C., Wang, C.-G. & Hsiao, Y.-S., 2003. Terrain correction computation using Gaussian quadrature, *Comput. Geosci.,* **29**(10), 1259–1268.

Jackson, J., 2002. Strength of the continental lithosphere: time to abandon the jelly sandwich? *GSA Today,* **12**(9), 4–10.

Jin, Y., McNutt, M. & Zhu, Y.S., 1996. Mapping the descent of Indian and Eurasian plates beneath the Tibetan Plateau from gravity anomalies, *J. geophys. Res,* **101**(B5), 11 275–11 290.

Jordan, T.A. & Watts, A.B., 2005. Gravity anomalies, flexure and the elastic thickness structure of the India–Eurasia collisional system, *Earth planet. Sci. Lett.,* **236**(3–4), 732–750.

Jouanne, F., Mugnier, J.L., Gamond, J.F., Le Fort, P., Pandey, M.R., Bollinger, L., Flouzat, M. & Avouac, J.P., 2004. Current shortening across the Himalayas of Nepal, *Geophys. J. Int.,* **157**(1), 1–14.

Karner, G. & Watts, A., 1983. Gravity anomalies and flexure of the lithosphere at mountain ranges, *J. geophys. Res.,* **88,** 10 449–10 477.

Karner, G.D., Steckler, M.S. & Thorne, J.A., 1983. Long-term thermomechanical properties of the continental lithosphere, *Nature,* **304,** 250–253.

Kumar, M.R., Saul, J., Sarkar, D., Kind, R. & Shukla, A.K., 2001. Crustal structure of the Indian Shield: new constraints from teleseismic receiver functions, *Geophys. Res. Lett.,* **28**(7), 1339–1342.

Kumar, P., Yuan, X., Kumar, M., Kind, R., Li, X. & Chadha, R., 2007. The rapid drift of the Indian tectonic plate, *Nature,* **449,** 894–897.

Langston, C., 1977. Corvallis, Oregon, crustal and upper mantle receiver structure from teleseismic P-waves and S-waves, *Bull. seism. Soc. Am.,* **67**(3), 713–724.

Larson, K.M., Burgmann, R., Bilham, R. & Freymueller, J.T., 1999. Kinematics of the India-Eurasia collision zone from GPS measurements, *J. geophys. Res.,* **104**(B1), 1077–1093.

Lave, J. & Avouac, J.P., 2000. Active folding of fluvial terraces across the Siwaliks Hills, Himalayas of central Nepal, *J. geophys. Res.,* **105**(B3), 5735–5770.

Lave, J. & Avouac, J.P., 2001. Fluvial incision and tectonic uplift across the Himalayas of central Nepal, *J. geophys. Res.,* **106**(B11), 26 561–26 591.

Le Fort, P., 1975. Himalaya: the collided range. Present knowledge of the continental arc., *Am. J. Sci.,* **275A,** 1–44.

Lyard, F., Lefèvre, F., Letellier, T. & Francis, O., 2006. Modelling the global ocean tides: a modern insight from fes2004, *Ocean Dyn.,* **56,** 394–415.

Lyon-Caen, H. & Molnar, P., 1983. Constraints on the structure of the Himalaya from an analysis of gravity-anomalies and a flexural model of the lithosphere, *J. geophys. Res.,* **88**(10), 8171–8191.

Lyon-Caen, H. & Molnar, P., 1985. Gravity-anomalies, flexure of the Indian Plate, and the structure, support and evolution of the Himalaya and Ganga Basin, *Tectonics,* **4**(6), 513–538.

Martelet, G., Sailhac, P., Moreau, F. & Diament, M., 2001. Characterization of geological boundaries using 1-D wavelet transform on gravity data: theory and application to the Himalayas, *Geophysics,* **66**(4), 1116–1129.

McKenzie, D. & Fairhead, D., 1997. Estimates of the effective elastic thickness of the continental lithosphere from Bouguer and free air gravity anomalies, *J. geophys. Res.,* **102**(B12), 27 523–27 552.

Monsalve, G., Sheehan, A., Rowe, C. & Rajaure, S., 2008. Seismic structure of the crust and the upper mantle beneath the Himalayas: evidence for eclogitization of lower crustal rocks in the Indian Plate, *J. geophys. Res.,* **113,** B08315, doi:10.1029/2007JB005424.

Mugnier, J.L. & Huyghe, P., 2006. Ganges basin geometry records a pre-15 Ma isostatic rebound of Himalaya, *Geology,* **34**(6), 445–448.

Nabelek, J. *et al.*, 2009. Underplating in the Himalaya-Tibet collision zone revealed by the Hi-CLIMB experiment, *Science,* **325**(5946), 1371–1374.

Nelson, K.D. *et al.*, 1996. Partially molten middle crust beneath southern Tibet: synthesis of project INDEPTH results, *Science,* **274**(5293), 1684–1688.

Pandey, O.P. & Agrawal, P.K., 1999. Lithospheric mantle deformation beneath the Indian cratons, *J. Geol.,* **107,** 683–692.

Raiverman, V., Kunte, S. & Mukherjea, A., 1983. Basin geometry, Cenozoic sedimentation and hydrocarbon prospects in north western Himalaya and Indo-Gangetic Plains, *Petrolog. Asian J.,* **11,** 67–92.

Ranalli, G., 1995. *Rheology of the Earth,* Springer.

Robert, X., van der Beek, P., Braun, J., Perry, C. & Mugnier, J.L., 2011. Control of detachment geometry on lateral variations in exhumation rates in the Himalaya: insights from low-temperature thermochronology and numerical modeling, *J. geophys. Res.,* **116,** B05202, doi:10.1029/2010JB007893.

Royden, L., 1993. The steady state thermal structure of eroding orogenic belts and accretionary prisms, *J. geophys. Res.,* **98**(B3), 4487–4507.

Sastri, V., Bhandari, L., Raju, A. & Datta, A., 1971. Tectonic framework and subsurface stratigraphy of the Ganga basin, *J. Geol. Soc. India,* **12**(3), 222–233.

Schulte-Pelkum, V., Monsalve, G., Sheehan, A., Pandey, M.R., Sapkota, S., Bilham, R. & Wu, F., 2005. Imaging the Indian subcontinent beneath the Himalaya, *Nature,* **435**(7046), 1222–1225.

Searle, M., 2010. Low-angle normal faults in the compressional Himalayan orogen: evidence from the Annapurna–Dhaulagiri Himalaya, Nepal, *Geosphere,* **6,** 296–315.

Sun, W., 1989. *Bouguer Gravity Anomaly Map of the People's Republic of China,* Chin. Acad. Geoexploration.

Tiwari, V., Rao, M., Mishra, D. & Singh, B., 2006. Crustal structure across Sikkim, NE Himalaya from new gravity and magnetic data, *Earth planet. Sci. Lett.,* **247,** 61–69.

Upreti, B.N., 1999. An overview of the stratigraphy and tectonics of the Nepal Himalaya, *J. Asian Earth Sci.,* **17**(5–6), 577–606.

Wenzel, H., 1996. The nanogal software: Earth tide data processing package ETERNA 3.3, *Bulletin d'Informations Marees Terrestres,* **124,** 9425–9439.

Wessel, P. & Smith, W. H.F., 1995. New version of the generic mapping tools, *EOS, Trans. Am. geophys. Un.,* **76**(33), 329.

Wittlinger, G., Farra, V., Hetényi, G., Vergne, J. & Nabelek, J., 2009. Seismic velocities in Southern Tibet lower crust: a receiver function approach for eclogite detection, *Geophys. J. Int.,* **177,** 1037–1049.

Won, I. & Bevis, M., 1987. Computing the gravitational and magnetic anomalies due to a polygon: algorithms and Fortran subroutines, *Geophysics,* **52,** 232–238.

Yin, A., 2006. Cenozoic tectonic evolution of the Himalayan orogen as constrained by along-strike variation of structural geometry, exhumation history, and foreland sedimentation, *Earth-Sci. Rev.,* **76**(1–2), 1–131.

Zhang, J., Santosh, M., Wang, X., Guo, L., Yang, X. & Zhang, B., 2012. Tectonics of the northern Himalaya since the India–Asia collision, *Gondwana Res.,* **21**(4), 939–960.

Zhang, Z. & Klemperer, S., 2010. Crustal structure of the Tethyan Himalaya, southern Tibet: new constraints from old wide-angle seismic data, *Geophys. J. Int.,* **181**(3), 1247–1260.

Zhao, W.J. & Nelson, K.D., 1993. Deep seismic-reflection evidence for continental underthrusting beneath Southern Tibet, *Nature,* **366**(6455), 557–559.